

# Illuminating the Mass Gap Through Deep Optical Constraint on a Neutron Star Merger Candidate S250206dm

ZHENGYAN LIU ,<sup>1, 2, \*</sup> ZELIN XU,<sup>1, 2, \*</sup> JI-AN JIANG ,<sup>1, 2, 3</sup> WEN ZHAO ,<sup>1, 2</sup> ZHIPING JIN ,<sup>4</sup> ZIGAO DAI ,<sup>1, 2</sup>  
 DEZHENG MENG,<sup>1, 2</sup> XUEFENG WU ,<sup>4</sup> DAMING WEI ,<sup>4</sup> RUNDUO LIANG ,<sup>1, 2, 5</sup> LEI HE ,<sup>1, 2</sup> MINXUAN CAI ,<sup>1, 2</sup>  
 LULU FAN ,<sup>1, 2, 6</sup> WEIYU WU,<sup>1, 2</sup> JUNHAN ZHAO,<sup>1, 2</sup> ZIQING JIA,<sup>1, 2</sup> KEXIN YU,<sup>1, 2</sup> JINJUN GENG ,<sup>4</sup> DI XIAO,<sup>4</sup>  
 FENG LI,<sup>7</sup> JINLONG TANG,<sup>8</sup> YINGXI ZUO,<sup>4</sup> XIAOLING ZHANG,<sup>4</sup> HAO LIU,<sup>7</sup> JIAN WANG ,<sup>6, 7</sup> HONGFEI ZHANG ,<sup>7</sup>  
 MING LIANG,<sup>9</sup> HAIREN WANG ,<sup>4</sup> DAZHI YAO,<sup>4</sup> LEI HU ,<sup>10, 4</sup> XU KONG ,<sup>1, 2, 6</sup> BIN LI ,<sup>4</sup> NING JIANG ,<sup>1, 2</sup>  
 TINGGUI WANG ,<sup>1, 2, 6</sup> ZHEN WAN ,<sup>1, 2</sup> YONGQUAN XUE ,<sup>1, 2</sup> QINGFENG ZHU ,<sup>1, 2, 6</sup> AND XIANZHONG ZHENG ,<sup>11</sup>

<sup>1</sup>Department of Astronomy, University of Science and Technology of China, Hefei 230026, China

<sup>2</sup>School of Astronomy and Space Sciences, University of Science and Technology of China, Hefei 230026, China

<sup>3</sup>National Astronomical Observatory of Japan, National Institutes of Natural Sciences, Tokyo 181-8588, Japan

<sup>4</sup>Purple Mountain Observatory, Chinese Academy of Sciences, Nanjing 210023, China

<sup>5</sup>National Astronomical Observatories, Chinese Academy of Sciences, Beijing 100101, China

<sup>6</sup>Institute of Deep Space Sciences, Deep Space Exploration Laboratory, Hefei 230026, China

<sup>7</sup>State Key Laboratory of Particle Detection and Electronics, University of Science and Technology of China, Hefei 230026, China

<sup>8</sup>Institute of Optics and Electronics, Chinese Academy of Sciences, Chengdu 610209, China

<sup>9</sup>National Optical Astronomy Observatory (NSF's National Optical-Infrared Astronomy Research Laboratory), 950 N Cherry Ave, Tucson Arizona 85726, USA

<sup>10</sup>McWilliams Center for Cosmology, Department of Physics, Carnegie Mellon University, 5000 Forbes Ave, Pittsburgh, 15213, PA, USA

<sup>11</sup>Tsung-Dao Lee Institute and Key Laboratory for Particle Physics, Astrophysics and Cosmology, Ministry of Education, Shanghai Jiao Tong University, Shanghai 201210, China

## ABSTRACT

The gravitational wave (GW) event S250206dm, as the first well-localized neutron star merger candidate potentially located in the mass gap, presented a unique opportunity to probe the electromagnetic signatures from such a system. Here we report a deep, multiband search with the new 2.5-meter Wide Field Survey Telescope (WFST), covering  $\sim$ 64% of the localization region up to a  $5\sigma$  limiting magnitude of 23 mag. In total, 12 potential candidates have been identified while none of them are likely related to S250206dm. This non-detection provides the most stringent constraint to date on any associated kilonova. Crucially, an AT 2017gfo-like event at 269 Mpc can be excluded only by WFST observations. Based on ejecta mass limits, a neutron star–black hole with a large mass ratio ( $Q \gtrsim 3.2$ ) is disfavored. This optical-derived constraint on the mass ratio reaches, for the first time, a precision comparable to that inferred from the GW signal. This work presents the best observation of this type of events until now, and demonstrates the power of rapid, deep follow-up observations to constrain the properties of compact binary progenitors, offering key insights into the constituents of the mass gap.

*Keywords:* Gravitational wave astronomy (675) — Neutron stars (1108)

## 1. INTRODUCTION

Binary neutron star (BNS) and neutron star–black hole (NSBH) mergers are gravitational wave (GW) sources, which can produce electromagnetic (EM) counterparts (B. P. Abbott et al. 2017a; B. D. Metzger 2020; E. Nakar 2020). As the first confirmed BNS merger, the GW event GW170817 (B. P. Abbott et al. 2017b), and the subsequent discovery of its EM counterparts marked a breakthrough, opening the era of multi-messenger astronomy. Various EM counterparts to GW170817 were observed across the entire EM spectrum by numerous facilities. Approximately two seconds post-

Corresponding author: Wen Zhao, Zhiping Jin, Zigao Dai  
 wzhao7@ustc.edu.cn, jin@pmo.ac.cn, daizg@ustc.edu.cn

\* These authors contributed equally to this work.

merger, the Fermi Gamma-ray Space Telescope detected the short gamma-ray burst (sGRB) GRB170817A, which lasted about two seconds (A. Goldstein et al. 2017; V. Savchenko et al. 2017). Subsequently, ultraviolet, optical, and near-infrared emissions were detected and confirmed as being from a kilonova (KN) coincident with GW170817 and GRB170817A, designated as AT2017gfo (D. A. Coulter et al. 2017; E. Pian et al. 2017; N. R. Tanvir et al. 2017; B. J. Shappee et al. 2017). The afterglow emissions were also detected later from X-ray to radio (E. Troja et al. 2017; P. D’Avanzo et al. 2018). The EM counterpart observations, combined with GW data, can be applied to a wide range of scientific studies, such as the origin of heavy elements and constraints on the Hubble constant (D. Kasen et al. 2017; B. P. Abbott et al. 2017).

KN is an approximately thermal transient powered by the radioactive decay of *r*-process nuclei, which has long been suspected to be generated in BNS or NSBH mergers (J. M. Lattimer & D. N. Schramm 1974; J. M. Lattimer et al. 1977; D. Eichler et al. 1989). The case of a BNS merger being the progenitor of a KN was confirmed by the multi-messenger detection of GW170817. To search for the KNe from NSBH mergers, many observations were conducted to follow up NSBH merger candidates during the third observing run (O3) of the LIGO Scientific and Virgo Collaboration (LVC) (K. Ackley et al. 2020; S. Anand et al. 2020). However, no evident KN from a NSBH merger has been found so far. The non-detection results can be attributed to several main reasons. Firstly, whether tidal disruption occurs in a NSBH merger is crucial for producing a KN. Secondly, KN is a faint and fast-evolving transient, requiring a timely and deep follow-up to search. Finally, due to the large localization area, it is difficult to cover the entire skymap even for wide-field telescopes, and searching for KN candidates is also challenging considering the numerous transients in survey data.

During O4, the LIGO/Virgo/KAGRA (LVK) Collaboration has detected a few GW events likely originating from BNS or NSBH mergers with low false alarm rates (FARs). For NSBH merger candidates, only two events, GW230529\_181500 and S250206dm, have a significant probability of retaining neutron star material outside the merger remnant, potentially producing an EM counterpart (A. G. Abac et al. 2024; Ligo Scientific Collaboration et al. 2025). Additionally, the source classifications of both events are uncertain. They may originate from either a BNS or a NSBH merger, with a high probability of involving one compact object in the so-called lower “mass gap” between the anticipated mass range ( $\sim 3$  to  $\sim 5 M_{\odot}$ ) of NSs and that of BHs. The detection of an EM counterpart is an effective way to infer the nature of the composition of the merging system (C. Barbieri et al. 2019; K. Kawaguchi et al. 2020). For GW230529\_181500, searching for its EM counterpart is challenging due to its poor localization, spanning a sky area of approximately  $24,100 \text{ deg}^2$  at the 90% credible level (A. G. Abac et al. 2024). S250206dm, detected on 6 February 2025, was localized to a 90% credible area of  $547 \text{ deg}^2$  (Ligo Scientific Collaboration et al. 2025). The relatively precise localization makes the event a rare opportunity to search for an EM counterpart of a NSBH merger.

In this paper, we present the follow-up campaign conducted by the 2.5-meter Wide Field Survey Telescope (WFST) for S250206dm. In Section 2, we introduce the GW event S250206dm and the follow-up observations by WFST. In Section 3, the procedures of data reduction and EM counterpart search are presented. The probability of discovered candidates as the EM counterpart is discussed in detail in Section 4. In Section 5, based on the non-detection result, the constraints on the potential KN and the progenitor of S250206dm are presented. The comparison with other follow-up campaigns and potential joint constraint are discussed in Section 6. Finally, we conclude our search campaign and constraint results in Section 7. Throughout this study, we adopt a standard  $\Lambda$ CDM cosmology with parameters  $H_0 = 67.7 \text{ km s}^{-1} \text{ Mpc}^{-1}$ ,  $\Omega_M = 0.31$  and  $\Omega_{\Lambda} = 0.69$  (Planck Collaboration et al. 2020).

## 2. S250206DM AND WFST FOLLOW-UP CAMPAIGN

The GW event S250206dm was detected by the LIGO-Livingston and LIGO-Hanford detectors at 21:25:30.439 UTC on February 6, 2025, when Virgo and KAGRA were offline<sup>12</sup>. After several alerts updated (Ligo Scientific Collaboration et al. 2025), S250206dm has a low FAR of 1 per 25.01 years and may originate from a BNS merger or a NSBH merger, with probabilities of 37% and 55%, respectively. The localization of S250206dm was estimated to have a median luminosity distance of 373 Mpc and a 90% skymap area of  $547 \text{ deg}^2$ . Other significant compact binary merger events detected in O4, which have at least one NS pre-merger, are listed in Table 1. The threshold of  $P_{\text{BNS}} + P_{\text{NSBH}} > 0.2$  is adopted to select events with at least one NS. For events with higher  $P_{\text{BBH}}$ , the systems have larger chirp masses and heavier BHs, where the NS is unlikely to be tidally disrupted unless the BH has a high

<sup>12</sup> <https://online.igwn.org>

aligned spin. According to the preliminary online estimates, for NSBH merger candidates, GW230529\_181500 and S250206dm are the most likely to produce EM counterparts, with  $P_{\text{HasRemnant}} > 0$  for the two events only. Given the more precise localization, S250206dm is more feasible for current wide-field survey facilities to follow up.

**Table 1. Properties of the significant BNS or NSBH candidates discovered in O4.** The information of these candidates is from GRACEDEB<sup>1</sup>, where the BNS or NSBH candidates are selected by  $P_{\text{BNS}} + P_{\text{NSBH}} > 0.2$ .

Event	FAR (/yr)	$P_{\text{BNS}}$	$P_{\text{NSBH}}$	$P_{\text{BBH}}$	$P_{\text{HasRemnant}}$	$A_{90}$ (deg $^2$ )	$D_{\text{L}}$ (Mpc)
S230518h	0.10	0%	86%	4%	0%	460	$204 \pm 57$
GW230529_181500 <sup>2</sup>	0.0062	31%	62%	0%	12%	24534	$197 \pm 62$
S230627c	0.10	0%	49%	48%	0%	82	$291 \pm 64$
S240910ci	0.10	0%	31%	69%	0%	394	$662 \pm 166$
S241109bn	$4.5 \times 10^{-4}$	0%	72%	28%	0%	10138	$603 \pm 159$
S250206dm	0.04	37%	55%	0%	30%	547	$373 \pm 104$
S250818k	2.15	29%	0%	0%	100%	949	$237 \pm 62$

<sup>1</sup> <https://gracedb.ligo.org/>

<sup>2</sup> Although the data of GW230529\_181500 has been released, the online results of the event property is adopted here to compare with other events.

We conducted a follow-up campaign for S250206dm using WFST, installed at the summit of the Saishiteng Mountain near Lenghu (L. Deng et al. 2021), Qinghai province, China. WFST has a field of view (FoV) of 6.55 deg $^2$  and a 2.5-meter primary mirror, making WFST one of the most powerful transient survey facilities in the world (T. Wang et al. 2023; G. Conroy 2023). Extragalactic transients are primary targets for WFST (T. Wang et al. 2023), including GW EM counterparts, supernovae, tidal disruption events, etc. WFST got the first light in September 2023, a few months after the start of O4. To search for potential EM counterparts of GW events detected in O4, a pre-research and delicate follow-up strategy through WFST target of opportunity (ToO) observations were developed in Z.-Y. Liu et al. (2023). The ToO strategy was subsequently applied to observations of GW events S240422ed and S250206dm.

**Table 2. The summary of WFST follow-up observations for S250206dm.**

Night	Start time (UTC)	End time (UTC)	Band	Area <sup>1</sup> (deg $^2$ )	$P_{\text{covered}}^1$
1	2025-02-07T12:10:10	2025-02-07T17:01:21	$r, i, z$	345	$\sim 64\%$
2	2025-02-08T12:14:53	2025-02-08T17:15:32	$r, i, z$	345	$\sim 64\%$
3	2025-02-09T12:14:04	2025-02-09T17:00:05	$r, i, z$	259	$\sim 63\%$
4			No observation due to weather		
5	2025-02-11T13:00:10	2025-02-11T16:49:24	$i, z$	97	$\sim 55\%$
6	2025-02-12T13:28:49	2025-02-12T17:06:47	$i, z$	85	$\sim 54\%$

<sup>1</sup> Corresponding to total covered area and probability of all bands, where the FoV of WFST is approximated as a circle with 1.4 $^{\circ}$  radius.

For S250206dm, WFST observations started approximately 14.7 hours (12:10 UTC on February 7, 2025) after the GW detection and lasted for a week (Z. Y. Liu et al. 2025; Z. L. Xu et al. 2025), primarily focused on the northern part of skymap. To mitigate the effects of moonlight (moon phase of  $\sim 0.7$ , increasing in subsequent nights) and Galactic extinction, a longer-wavelength combination of  $r$ ,  $i$ , and  $z$  bands was adopted. Additionally, given the high density of stars in the low Galactic latitude region of S250206dm skymap, exposure times of  $1 \times 90$  s and  $2 \times 60$  s for each pointing each band were adopted to prevent excessive saturation. For pointings with multiple coverages per night, they were dithered to fill the CCD gap.

The WFST coverage and limiting magnitudes on the first night are shown in Figure 1. To evaluate the search capability, the limiting magnitudes in each band are converted to absolute magnitudes using the median distance

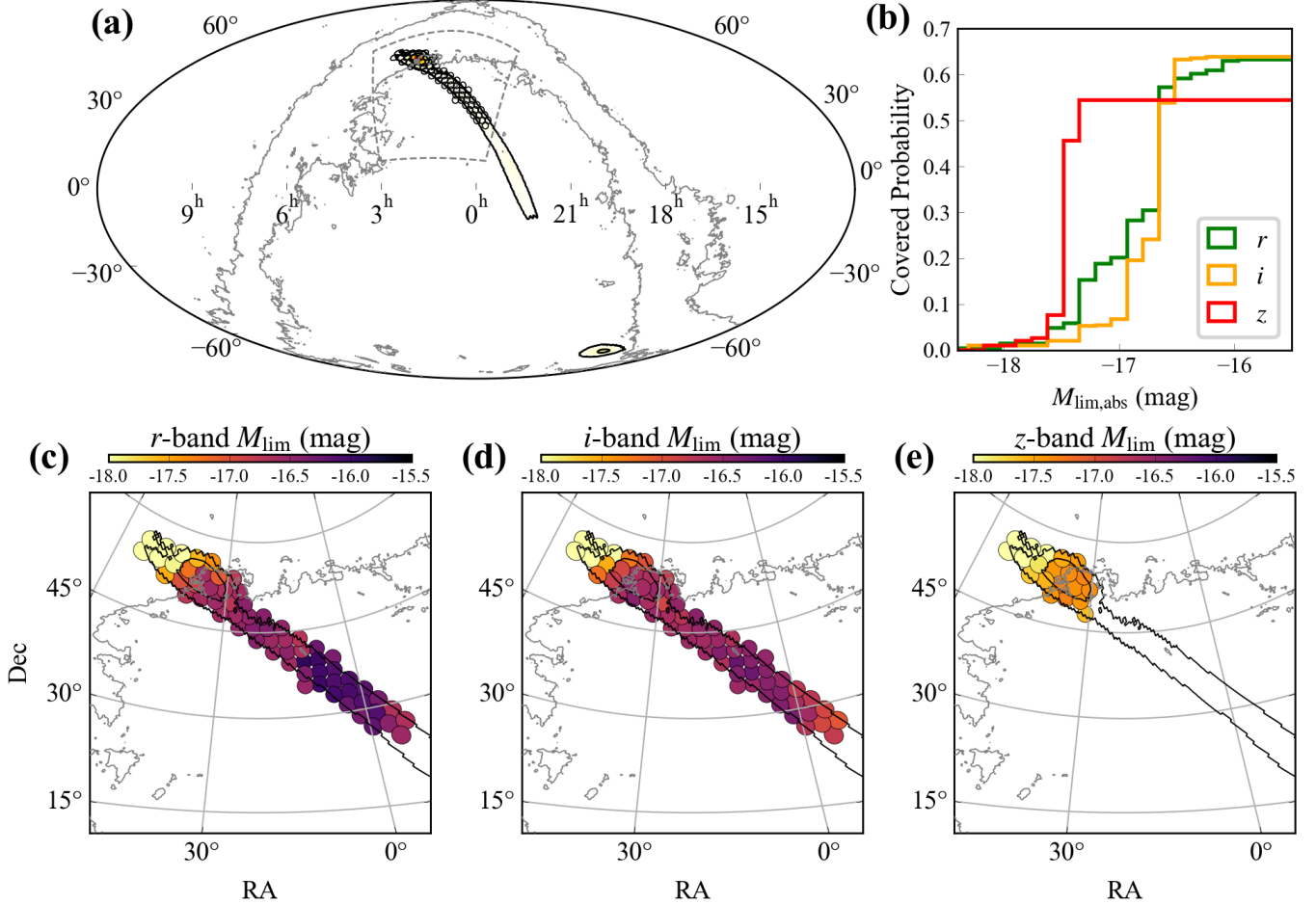


**Figure 1.** Skymap coverage and multiband depths of WFST on the first night for S250206dm. Panel (a): the total coverage by WFST for S250206dm, where the Bilby skymap of S250206dm from [Ligo Scientific Collaboration et al. \(2025\)](#) is adopted, with 50% and 90% probability region contours. Galactic extinction is also considered, with the contour of  $E(B - V) = 0.3$  for reference ([E. F. Schlafly & D. P. Finkbeiner 2011](#)). Panel (b): The probability coverage by the WFST as a function of limiting absolute magnitudes in  $r$ ,  $i$ , and  $z$  bands. Panel (c), (d), and (e): The zoomed-in covered regions by WFST in  $r$ ,  $i$ , and  $z$  bands, respectively, corresponding to the region delineated by the dashed line in Panel (a). The color map represents the 5 $\sigma$  limiting absolute magnitudes after stacking, converted based on the distance estimate for each WFST pointing.

estimate from the GW skymap in Panel (c), (d), and (e). The effect of Galactic foreground extinction is also included. The host extinction is not considered in this work due to the generally large projected distance from galactic center ([W.-f. Fong et al. 2022](#)). The extinction correction in this work is based on  $E(B - V)$  map from [E. F. Schlafly & D. P. Finkbeiner \(2011\)](#), with  $R_V = 3.1$ . For KN AT 2017gfo, the peak absolute magnitudes are approximately  $-16$  mag in  $r$ ,  $i$ , and  $z$  bands ([B. P. Abbott et al. 2017a](#)). With a limiting magnitude range from  $-15.8$  mag to  $-18.0$  mag approximately, our observations achieve the depth required to detect an AT 2017gfo-like KN at the peak phase.

The observing strategies for the second and third nights were similar to that of the first night. As the potential KN became fainter and the localization was updated, a strategy with a longer exposure time and a smaller coverage area was adopted. Specifically, for the fifth and the sixth nights, the reduced coverage region is shown in Figure 2, where  $i$  and  $z$  bands with exposure times of  $3 \times 120$  s and  $2 \times 180$  s were used, respectively. The observation on the fourth night was not conducted due to snowy weather at the summit. The covered area, probability, and observation time range for each night are summarized in Table 2. In total,  $\sim 64\%$  and  $\sim 55\%$  Bilby skymap ([Ligo Scientific Collaboration et al. 2025](#)) were covered by WFST in the first three nights and the last two nights, respectively.

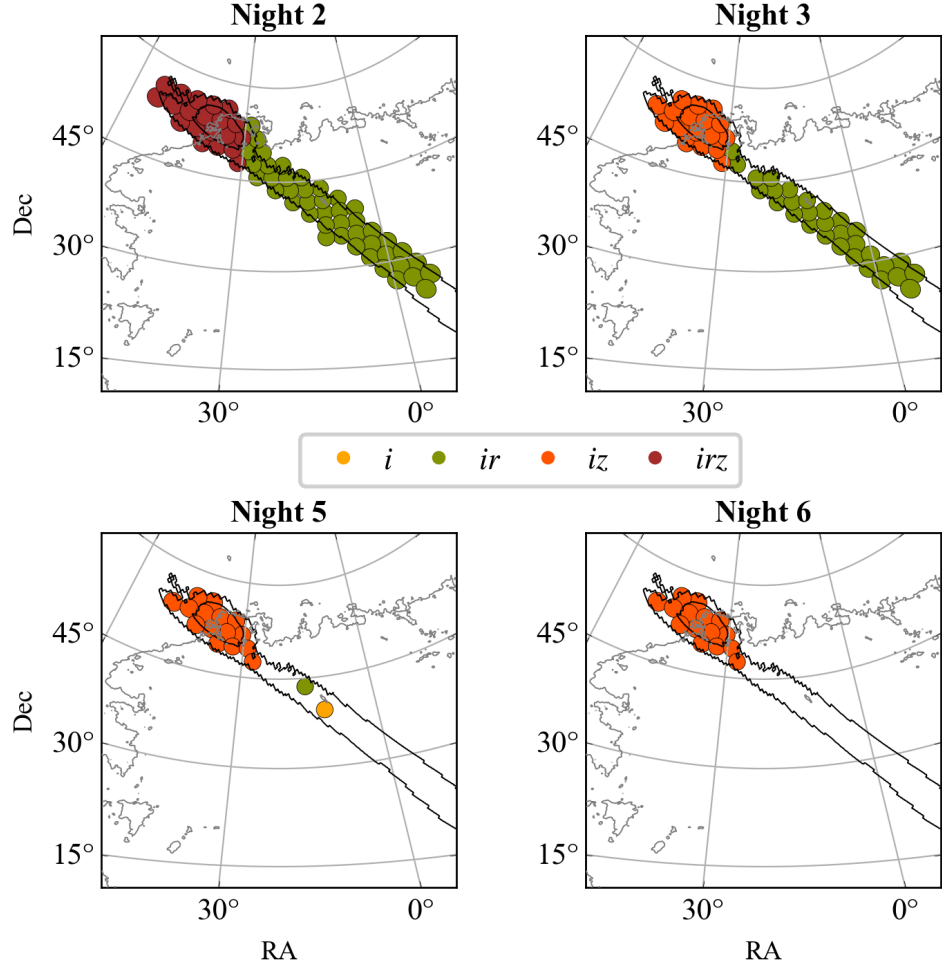


**Figure 2.** Skymap coverage of WFST observations for S250206dm after the first night. The Bilby skymap of S250206dm from [Ligo Scientific Collaboration et al. \(2025\)](#) is adopted, with 50% and 90% probability region contours shown. Galactic foreground is shown as a contour of  $E(B - V) = 0.3$  ([E. F. Schlafly & D. P. Finkbeiner 2011](#)).

### 3. SEARCH FOR EM COUNTERPART

The raw images from the follow-up observations of S250206dm were processed using the WFST pipeline, which is mainly based on the the Vera C. Rubin observatory (VRO/LSST) image processing pipeline (hereafter the “LSST pipeline”) ([J. Bosch et al. 2018](#)). The LSST pipeline is a modular and efficient software suite written in a combination of Python and C++ to process massive survey data. The main processing steps of the LSST pipeline include data ingestion, instrument signature removal, point spread function (PSF) modeling, astrometric and photometric calibration, source detection and deblending, image alignment and coaddition, image subtraction, and alert product generation. The WFST pipeline was modified from the LSST pipeline in two main aspects: the addition of extension files defining the CCD configuration and the replacement of the subtraction software with SFFT to optimize and expedite the subtraction process ([L. Hu et al. 2022](#)). Please see [M. Cai et al. \(2025\)](#) for details of the WFST pipeline.

To search for the EM counterpart timely, although the lack of WFST archival images for the S250206dm skymap, the preliminary search was conducted using the first night data as reference images, but no valid candidate was found. To ensure that the potential counterpart is faint enough, reference images were taken about two weeks later (2025-02-16T12:44 to 2025-02-21T14:59 UTC), millions of alerts were detected through basic image reduction, stacking for the images in the same band each night, and subtraction using the WFST pipeline. We searched for the KN using the following filtering criterias to exclude the contamination:

**Table 3.** The number of alert after series of filters for candidate search.

Description	Filter	Alert number
Total		3746535
Multiple detections	$N_{\text{det}} \geq 2$	1735634
Real source	$S_{\text{RB}} \geq 0.1$	93180
Positive source	$N_{\text{negative}} = 0$	48771
Not variable star	$d_{\text{point}} \geq 1''$	5002
Far from bright source	$d_{15\text{mag}} \geq 10'', d_{12\text{mag}} \geq 40''$	2236
Not galactic nucleus activity	$d_{\text{nuc}} \geq 0.5''$	2172
Not moving object	$d_{\text{SkyBot}} \geq 3''$	2172

1. Not bogus or artifacts: Require multiple detections of  $N_{\text{det}} \geq 2$  and  $S_{\text{RB}} \geq 0.1$ , where  $S_{\text{RB}}$ , calculated by a real-bogus (RB) classifier (Y. Liu et al. 2025), represents the fraction of real detections for an alert.
2. Not variable stars: Exclude alerts close to known point sources.
3. Not close to bright sources: Exclude alerts around bright sources ( $M < 15$  mag), which may produce false detections due to saturation.
4. Not galactic nucleus activity: Exclude alerts close to centers of known galaxies.
5. Not moving object: Exclude alerts close to known solar system objects.

The number of alerts remained after each filter is shown in Table 3, where crossmatches of variable stars, bright sources and galactic centers are preformed using Pan-STARRS1 (PS1) DR2 and Gaia DR3 catalogs (K. C. Chambers et al. 2016; Eugene. A. Magnier et al. 2020; Gaia Collaboration et al. 2023). Point and extended sources are distinguished by star classification probability and the difference between results of PSF and Kron photometry (with sources satisfying  $M_{i,\text{PSF}} - M_{i,\text{Kron}} < 0.05$  classified as stars<sup>13</sup>) for the Gaia and PS1 databases, respectively. To exclude moving objects, the remaining alerts were crossmatched with Sky Body Tracker to rule out Solar System objects (J. Berthier et al. 2006). Finally, 2172 alerts remained after applying an inclusive set of filters to avoid missing potential candidate. These remaining alerts will undergo visual inspection based on analogous criteria described in Table 3 to exclude artifacts and other contamination.

#### 4. CANDIDATE ANALYSIS

After visual inspection for the filtered alerts, 12 candidates were identified as off-nucleus extragalactic transients, as listed in Table 4. To exclude transients occurred before the GW detection, these candidates were crossmatched with public survey databases, including Transient Name Server (TNS; A. Gal-Yam 2021), Zwicky Transient Facility (ZTF; E. C. Bellm et al. 2019; M. J. Graham et al. 2019) ALeRCE explorer (F. Förster et al. 2021), and the Asteroid Terrestrial-impact Last Alert System (ATLAS; J. L. Tonry et al. 2018; K. W. Smith et al. 2020) forced photometry server (L. Shingles et al. 2021). Two candidates are excluded as potential counterparts due to archival detections by ZTF. Additionally, assuming the nearest galaxy as the host galaxy, the luminosity distances of remaining 10 candidates were obtained from the galaxy redshifts by crossmatching with the GLADE+ catalogs and PS1-based photometric redshift catalogs (R. Beck et al. 2021; G. Dálya et al. 2022). The percentiles of the marginal cumulative distribution function (CDF) at the locations of candidates are listed in Table 4, with four candidates excluded due to significantly larger distances compared with GW localization even when uncertainties of photometric redshifts are taken into account. For the 12th candidate, the subtraction was re-preformed with the archival images of PS1 3 $\pi$  survey as reference (R. Beck et al. 2021), due to that it is still visible in the WFST template images.

For the remained six candidates, we further compared their absolute magnitudes and variability (after Galactic extinction correction) with the KN model. The WFST lightcurves of the six candidates are shown in Figure 3. The peak absolute magnitudes and evolution of these candidates are shown in Figure 4. The spaces of KNe based on the model POSSIS (M. Bulla 2019; S. Anand et al. 2020; M. Bulla 2023) are shown for comparison (details of the

<sup>13</sup> <https://outerspace.stsci.edu/display/PANSTARRS/How+to+separate+stars+and+galaxies>

**Table 4.** Properties of 12 candidates after human vetting and specific reasons for exclusion as a KN counterpart.

No.	$N_{\text{det}}^1$	Ra	Dec	$\dot{M}_i^2$ (mag/day)	Band	$M_{i,\text{p}}^2$ (mag)	$M'_{i,\text{p}}^3$ (mag)	$D_{\text{L,host}}^4$ (Mpc)	$\text{CDF}(D_{\text{L}})^5$ (Kpc)	Reason
1	7	40.01920	50.88298	0.08 ± 0.03	$r, i, z$	-16.7 ± 0.5	-17.4 ± 0.5	395 ± 75 <sup>b</sup>	0.63	7.5
2	4	356.20086	28.06492	0.22 ± 0.11	$r, i$	-19.2 ± 0.1	-19.4 ± 0.1	446	0.54	5.5
3	4	35.91705	53.46289	0.02 ± 0.03	$i$	-18.6 ± 0.3	-19.0 ± 0.3	780 ± 81 <sup>a</sup>	0.94	15.2
4	4	30.12691	48.66882	0.00 ± 0.03	$i$	-18.3 ± 0.7	-18.7 ± 0.7	705 ± 203 <sup>a</sup>	0.99	2.7
5	4	29.93754	51.35800	-0.02 ± 0.03	$i$	-18.1 ± 0.7	-18.5 ± 0.7	589 ± 193 <sup>a</sup>	0.98	4.1
6	3	30.88382	49.36016	0.14 ± 0.07	$i$	-19.1 ± 0.7	-19.6 ± 0.7	990 ± 225 <sup>a</sup>	1.00	4.5
7	3	38.80782	56.26273	-0.05 ± 0.05	$i$	-17.3 ± 0.4	-18.5 ± 0.4	473 ± 76 <sup>a</sup>	0.86	7.1
8	2	3.45112	32.29102	0.03 ± 0.11	$i$	-17.1 ± 0.4	-17.2 ± 0.4	471 ± 76 <sup>a</sup>	0.62	4.7
9	2	4.47506	32.98365	-0.02 ± 0.12	$i$	-17.3 ± 0.5	-17.4 ± 0.5	472 ± 76 <sup>a</sup>	0.64	1.2
10	2	40.15301	53.50889	0.02 ± 0.03	$i$	-20.5 ± 0.6	-21.4 ± 0.6	2158 ± 504 <sup>b</sup>	1.00	3.5
11	3	32.21519	53.05843	0.03 ± 0.03	$i$	-20.6 ± 0.5	-21.0 ± 0.5	1789 ± 377 <sup>b</sup>	0.99	3.4
12	12	35.70140	50.28884	0.03 ± 0.01	$r, i, z$	-20.4 ± 0.6	-21.05 ± 0.6	1727 ± 375 <sup>b</sup>	0.99	4.4

<sup>1</sup> Total number of detections of each candidate, after stacking of images with same band each night. All uncertainties are given at the  $1\sigma$  level.

<sup>2</sup> The magnitude changing rate and peak absolute magnitude of each candidate are listed in  $i$  band. The error of peak absolute magnitudes include the uncertainties of the host distances.

<sup>3</sup> The peak absolute magnitude of each candidate after Galactic extinction correction.

<sup>4</sup> The spectroscopic redshift result of No. 2 candidate is from DESI DR1 (D. Collaboration et al. 2025). Distance with marker ‘a’ is based on the photometric redshifts collected in GLADE+ catalog (G. Dálya et al. 2022). If there is no match with GLADE+ catalog, the host distance is based on photometric redshift result of PS1 survey (R. Beck et al. 2021), and is marked with ‘b’.

<sup>5</sup> The cumulative conditional probability given the host distance and the candidate 2D location, based on the Bily sky map. For candidates excluded by ‘Skymap mismatched’, the host distance of  $\mu - 3\sigma$  is adopted to show the deviation considering uncertainty of photometric redshifts.

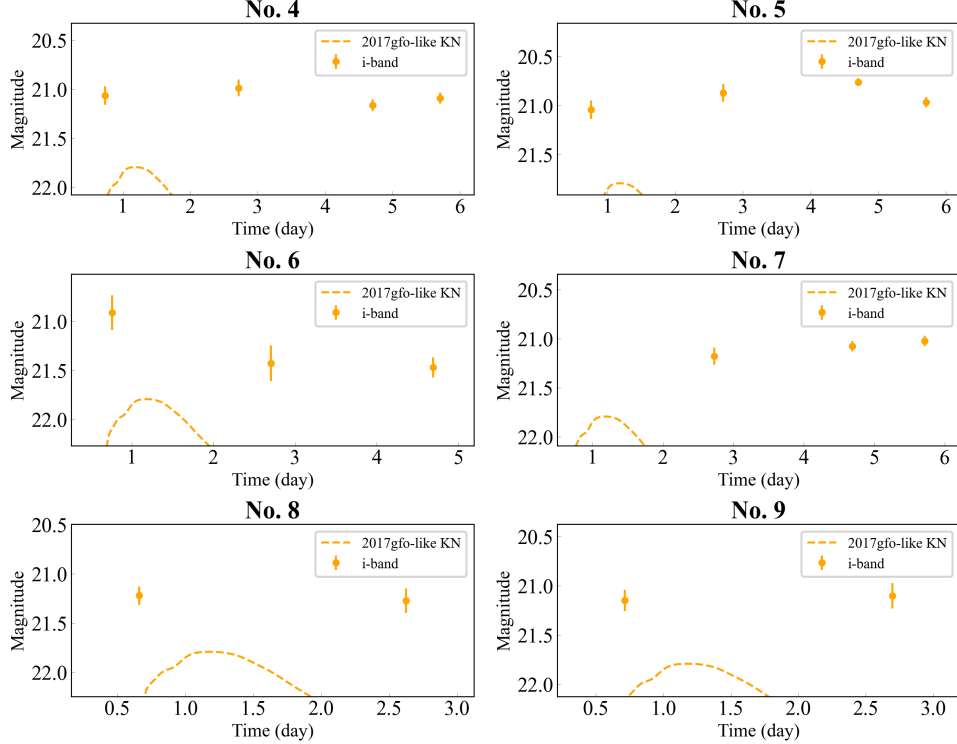


**Figure 3.** Lightcurves of the six WFST candidates tagged by “Too bright” or “Slow evolution”. The luminosity distance of a 2017gfo-like KN is set as the median of 373 Mpc.

model please see Section 5). The sampling times of simulated KN lightcurves used to derive absolute magnitudes and variability are  $\sim 0.7$  and  $\sim 2.7$  days post-merger, corresponding to the detection times of most candidates. Regarding their evolution, the decay rates of these six candidates are slower than those of KNe produced by BNS mergers but consistent with the range of decay rates for NSBH mergers. In terms of luminosity, all candidates are brighter than the luminosity range derived from the model, where the luminosity distance is set as 373 Mpc due to no spectroscopic redshift available for these candidates. Two candidates (the 8th and 9th) have peak magnitudes close to those of the simulated KN sample when the uncertainty of their photometric redshifts is considered. However, it remains challenging to classify them as KN candidates due to their limited number of detections. For other candidates, to produce such a bright KN, additional energy sources beyond radioactive decay are required, such as central engine activity (Y.-W. Yu et al. 2013). Some magnetar-enhanced KN candidates associated with short gamma-ray bursts were discovered (H. Gao et al. 2017), but no valid enhanced KN has been confirmed to date. Additionally, the merger remnant of S250206dm is unlikely to be a magnetar in the case of BNS merger due to its large chirp mass, which tends to collapse directly into a BH.

To analyze the possibility as the afterglow counterpart of S250206dm for these six candidates, the scenarios of the BNS and NSBH merger are discussed as follows, respectively. For a BNS merger, the afterglow lightcurves with various viewing angles are simulated using the model `afterglowpy` (G. Ryan et al. 2020), where the best-fitting results in G. Ryan et al. (2020) of the GRB 170817A afterglow are adopted for other model parameters. Producing an afterglow with similar luminosity to the candidates requiring a small viewing angle ( $\theta_{\text{obs}} < 3^\circ$ ), but the evolution of such afterglow is quite fast compared with the candidate lightcurves. For a NSBH merger, if these candidates originated from the afterglow, their slow evolutions correspond to the afterglow peak phase. According to:

$$t_{\text{peak},i} \simeq 1.2 \times 10^3 (1+z) \left( \frac{E_{\text{K},i}}{10^{53} \text{ erg}} \right)^{(1/3)} \left( \frac{n}{1 \text{ cm}^{-3}} \right)^{(-1/3)} \left( \frac{\Gamma_i}{50} \right)^{(-8/3)} \text{ s}, \quad (1)$$

$t_{\text{peak},i} \approx 2$  days corresponds to a slow Lorentz factor ( $\Gamma_i < 5$ ), where  $E_{\text{K},i} = 10^{55}$  erg and  $n = 0.1 \text{ cm}^{-3}$  (B. Zhang 2018). However, such a slow Lorentz factor is inconsistent with a jet from a NSBH merger due to a limited baryon loaded. Therefore, these six candidates are unlikely related to the KN or afterglow counterpart of S250206dm. No

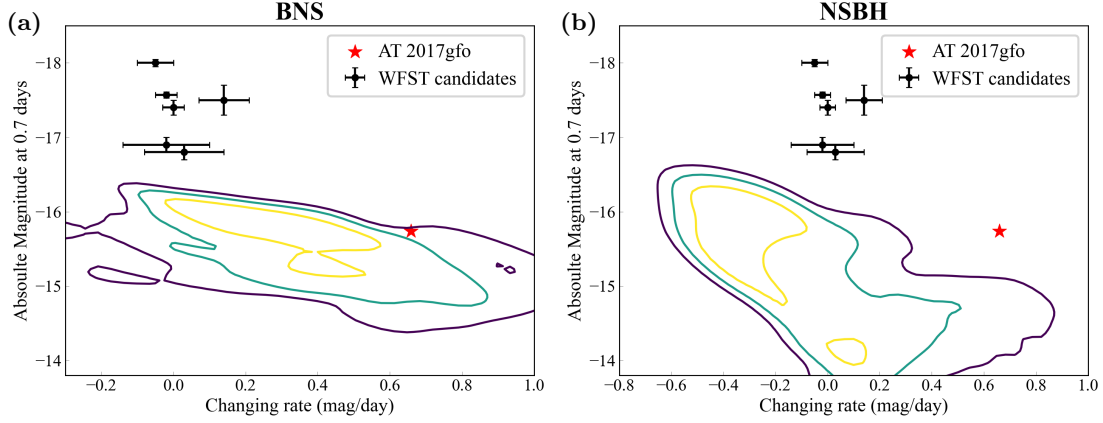


**Figure 4.** The model-dependent space of peak magnitude and variability in  $i$  band. Panel (a) and (b): The KN model POSSIS is adopted for simulating KNe in the BNS and NSBH mergers, respectively. The black dots and red pentacles represent the six candidates tagged by “Too bright” or “Slow evolution” and AT 2017gfo, respectively. To derive the absolute magnitude, the luminosity distance is set as 373 Mpc for the candidates with no spectroscopic redshift available. Three contour lines correspond to 50%, 90%, 99% percentiles of KN model regions.

spectral follow-up was carried out to further confirm the 12 candidates due to their faint brightnesses (mostly  $> 21$  mag) and reasons for exclusion.

Candidates reported in the community were also checked in WFST data. These candidates in the optical band are from the ZTF team (T. Ahumada et al. 2025) and TNS<sup>14</sup>. Candidates reported by the GW MultiMessenger Astronomy Dark Energy Camera (DECam; B. Flaugher et al. 2015) Survey team (L. Hu et al. 2025) are not included due to limited overlap in the covered regions between WFST and Wendelstein. The coverage and detection of candidates by WFST are listed in Table 6 in the appendix, where candidates reported before the GW detection time and with  $\text{Dec} \leq 0^\circ$  are not included. It is not surprising that most candidates were not detected in the WFST difference images due to the short time interval of approximately two weeks between the science and the reference images. Based on this time interval, the WFST follow-up observations are not sensitive to sources with slow evolution. For example, the candidate AT 2025bay, reported by ZTF, has a magnitude difference of  $\sim 0.2$  mag in  $r$  band between the time of obtaining WFST science images and that of reference images, according to the lightcurve in T. Ahumada et al. (2025). This variability, corresponding to  $\sim 22.5$  mag in WFST difference images, is near the detection limit of WFST. Such sources with slow evolution are faint and difficult to be detected in the WFST observations. Based on WFST detections, no candidate is likely to be the KN counterpart. Additionally, in the X-ray band, candidates reported by the Einstein Probe through GCN Circulars (D. Y. Li et al. 2025) were also checked in our data. However, no valid extragalactic source was discovered within the positional error of the candidates. Consequently, no robust KN candidate was discovered in the WFST follow-up observations.

## 5. COUNTERPART CONSTRAINT & INSIGHTS INTO ORIGIN

Although non-detection of EM counterpart of GW events, the KN luminosity, ejecta mass during merger, and merger system property can be constrained by follow-up observations assuming a KN model (M. M. Kasliwal et al. 2020; S. Anand et al. 2020; K. Ackley et al. 2020; M. Pillas et al. 2025). A state-of-art KN model POSSIS is adopted in our analysis. POSSIS is a radiative transfer code for KNe developed by M. Bulla (2019), including dynamical ejecta produced by collisions and tidal interactions, as well as disk wind ejecta generated by outflows from the post-merger accretion disk. For a BNS merger, post-merger ejecta and dynamical ejecta are distributed near the polar axis and the equatorial plane, respectively. As the grid model is based on simulations, the velocity ranges of dynamical and post-merger ejecta are fixed at  $0.1\text{--}0.3 c$  and  $0.025\text{--}0.1 c$ , respectively. The free parameters of the model include dynamical ejecta mass  $M_{\text{dyn}}$ , post-merger ejecta mass  $M_{\text{pm}}$ , half-opening angle of the dynamical ejecta  $\theta_{\text{open}}$  and viewing angle  $\theta_{\text{obs}}$ . A surrogate model from K. Lukošiute et al. (2022) is adopted to obtain results for arbitrary parameters in our calculations.

<sup>14</sup> [https://www.wis-tns.org/ligo/o4/S250206dm\\_20250206\\_212530](https://www.wis-tns.org/ligo/o4/S250206dm_20250206_212530)

For AT 2017gfo-like KNe, the lightcurves are produced using **POSSIS** with the parameters from the fitted results in [T. Dietrich et al. \(2020\)](#):  $M_{\text{dyn}} = 0.005 M_{\odot}$ ,  $M_{\text{pm}} = 0.052 M_{\odot}$ ,  $\theta_{\text{open}} = 49.5^\circ$ , and  $\theta_{\text{obs}} = 42.8^\circ$ . For general BNS mergers, the ranges of dynamical ejecta  $M_{\text{dyn}}$  and post-merger ejecta  $M_{\text{pm}}$  are 0.0025 to 0.02  $M_{\odot}$  and 0.01 to 0.1  $M_{\odot}$ , respectively. For NSBH mergers, the ranges of  $M_{\text{dyn}}$  and  $M_{\text{pm}}$  are both 0.01 to 0.09  $M_{\odot}$ . For BNS and NSBH mergers,  $\theta_{\text{open}}$  are fixed at  $45^\circ$  and  $30^\circ$  according to [M. Bulla \(2019\)](#) and [S. Anand et al. \(2020\)](#), respectively, and  $\theta_{\text{obs}}$  are both sampled uniformly. Additionally, the distance and the viewing angle are randomly combined in our analysis due to the lack of further estimate from the GW signal.

For a BNS merger origin, the constraint results based on **POSSIS** are shown in left two panels of Figure 5. As shown in the top-left panel of Figure 5, lightcurves of the AT 2017gfo-like KN and other simulated KNe from various parameter combinations are compared with WFST detection upper limits after considering Galactic extinction. The constraint mainly depends on observations of the first three nights due to the fast evolution for KNe from BNS mergers. At 269 Mpc, an AT 2017gfo-like KN can be ruled out by our observations in both  $r$  and  $i$  bands and most parameter combinations can also be excluded. The corresponding ejecta mass of the excluded lightcurves are shown in the bottom-left panel of Figure 5. As the viewing angle ( $\theta_{\text{obs}}$ ) or distance ( $D_L$ ) increases, KNe become fainter, leading to a broader range of allowed ejecta masses. Based on the ejecta mass estimate of AT 2017gfo ([T. Dietrich et al. 2020](#)), an AT 2017gfo-like KN is ruled out at 269 Mpc with viewing angle  $\theta_{\text{obs}} < 45^\circ$ . At  $\theta_{\text{obs}} = 45^\circ$  and  $D_L = 269$  Mpc, the masses of post-merger and dynamical ejecta are constrained to  $M_{\text{pm}} \lesssim 0.03 M_{\odot}$  and  $M_{\text{dyn}} \lesssim 0.01 M_{\odot}$ , respectively. These mass upper limits are consistent with the ejecta produced in a scenario that a BNS merger directly collapses into a BH.

For a NSBH merger origin, similar results to BNS are also shown in right two panels of Figure 5. KN lightcurves with bright peaks but rapid decay or faint peaks but slow decay are ruled out by the first and the fifth night observations, respectively. The WFST observations can effectively constrain KN lightcurves up to the median distance of 373 Mpc. As shown in the bottom-right panel of Figure 5, at  $\theta_{\text{obs}} = 45^\circ$  and  $D_L = 269$  Mpc, a total ejecta mass greater than  $\sim 0.1 M_{\odot}$  is ruled out. In the optimistic scenario ( $\theta_{\text{obs}} = 15^\circ$ ,  $D_L = 269$  Mpc), the masses of post-merger and dynamical ejecta can be further constrained to  $M_{\text{pm}} \lesssim 0.03 M_{\odot}$  and  $M_{\text{dyn}} \lesssim 0.03 M_{\odot}$ , respectively.

In comparison with **POSSIS**, we also employ another KN model **SuperNu** for the NSBH merger. **SuperNu** is a Monte Carlo radiative transfer code ([R. T. Wollaeger et al. 2019, 2021](#); [O. Korobkin et al. 2021](#)), assuming a two-component axisymmetric ejecta that includes dynamical and wind ejecta (similar to poster-merger ejecta in **POSSIS**, hereafter also referred to as post-merger ejecta). A grid of simulation results is calculated using **SuperNu** with varying masses, velocities, morphologies, and compositions. In our calculations, a surrogate model for **SuperNu** from [A. Kedia et al. \(2023\)](#) is adopted. Similar to the NSBH case in **POSSIS**, a morphology (named “TSwind2” in [A. Kedia et al. \(2023\)](#)) is adopted for KNe produced by a NSBH merger, including a torus-shaped dynamical ejecta and a spherical post-merger ejecta. To reduce the model’s degrees of freedom, the velocities of the dynamical and post-merger ejecta are set to  $0.18 c$  and  $0.06 c$ , respectively, corresponding to the average velocities derived from the velocity distribution of the **POSSIS** NSBH model. The ejecta mass ranges for the two components are both 0.01 to 0.09  $M_{\odot}$ . The constraint results, similar to those in Figure 5, are shown in Figure 6. Compared with **POSSIS**, the trends of the results are similar, and the constraints weaken as the distance or viewing angle increases. For **SuperNu**, the KN lightcurves are more sensitive to  $M_{\text{pm}}$ : at a distance of 269 Mpc and a viewing angle of  $45^\circ$ ,  $M_{\text{pm}} < 0.03 M_{\odot}$  is derived from our observational upper limits, but with no effective constraint on  $M_{\text{dyn}}$ . Overall, the constraint on  $M_{\text{pm}}$  is tighter than that for **POSSIS**, whereas the opposite holds for  $M_{\text{dyn}}$ .

Combined with the numerical simulation results of BNS and NSBH mergers, the derived constraints on ejecta mass can be used to further infer the properties of the progenitor ([I. Andreoni et al. 2020](#); [M. W. Coughlin et al. 2020](#); [S. Anand et al. 2020](#)). For a BNS merger origin for S250206dm, a large chirp mass leads to direct collapse into a BH during the merger. It is challenging to infer the merger system due to the theoretically small amount of ejecta. Therefore, we consider only the NSBH merger case here. The empirical equations from numerical simulation results, as used in [B. P. Gompertz et al. \(2023\)](#) and [M. Pillas et al. \(2025\)](#), are adopted here to derive  $M_{\text{dyn}}$  and  $M_{\text{pm}}$  for the progenitor. Specifically, Equation 9 in [C. J. Krüger & F. Foucart \(2020\)](#) is used to calculate  $M_{\text{dyn}}$ . The total ejecta mass,  $M_{\text{rem}}$ , is estimated using Equation 4 in [F. Foucart et al. \(2018\)](#), where  $M_{\text{rem}} = M_{\text{disk}} + M_{\text{dyn}}$ . The post-merger (wind) ejecta mass is obtained by a fraction  $\xi$  of disk material converted into wind ejecta, where  $\xi$  is related to the binary mass ratio and can be estimated using Equation 12 in [G. Raaijmakers et al. \(2021\)](#). In our calculations, the H4 and APR EoSs are adopted, with their  $R_{1.4}$  and  $M_{\text{TOV}}$  values being (13.7 km,  $2.03 M_{\odot}$ ) and (11.3 km,  $2.19 M_{\odot}$ ), representing a “stiff” and a “soft” EoS, respectively.

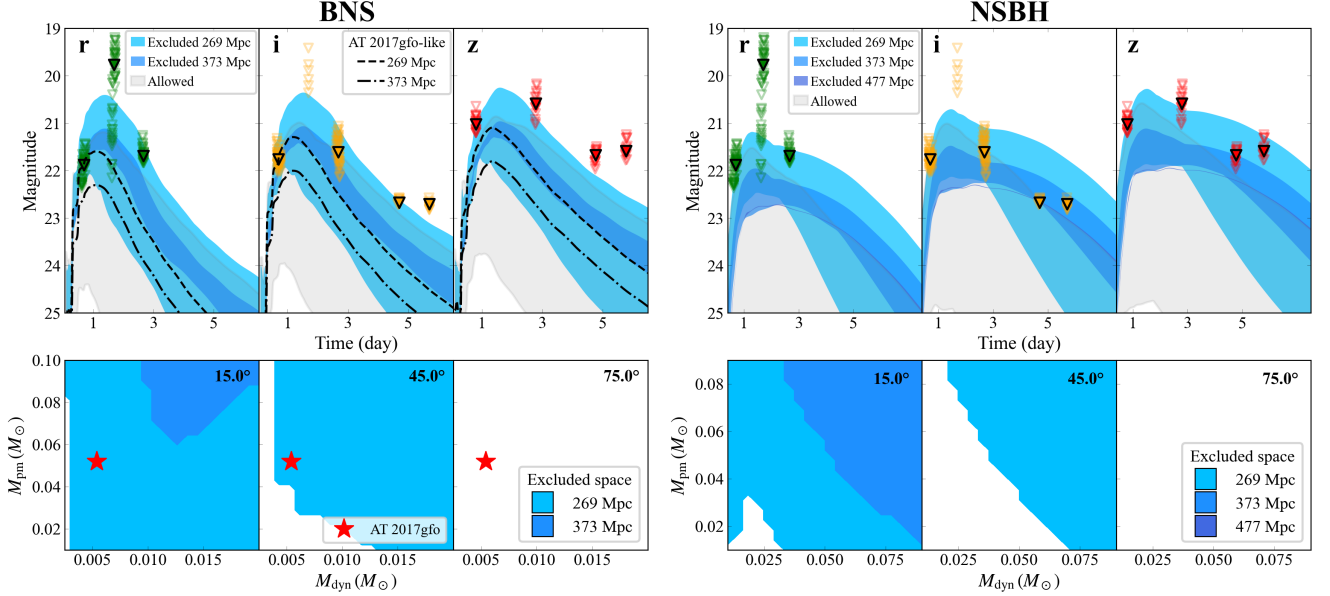


**Figure 5.** Parameters constraints based on the non-detection result, assuming a BNS (left) or a NSBH merger (right) for S250206dm. Two top panels show constraints on KN luminosity derived using the POSSIS model at different distances (corresponding to the median and  $\pm 1\sigma$  distances from Bilby skymap). The  $5\sigma$  limiting magnitude of each WFST pointing and the median magnitudes are plotted with open and solid inverted triangles, respectively. Galactic extinction with a median  $E(B - V) = 0.1$  is applied in all panels. Light/deep blue and gray regions represent excluded and allowed KN scenarios, respectively. For the BNS merger, black dashed and dash-dot lines represent AT 2017gfo-like KNe generated using POSSIS at 269 and 373 Mpc, respectively. Two bottom panels show constraints on ejecta mass. Three viewing angles of  $15^\circ$ ,  $45^\circ$  and  $75^\circ$  are adopted. The fitted ejecta masses of AT 2017gfo from T. Dietrich et al. (2020) are plotted as a red star for the BNS merger.

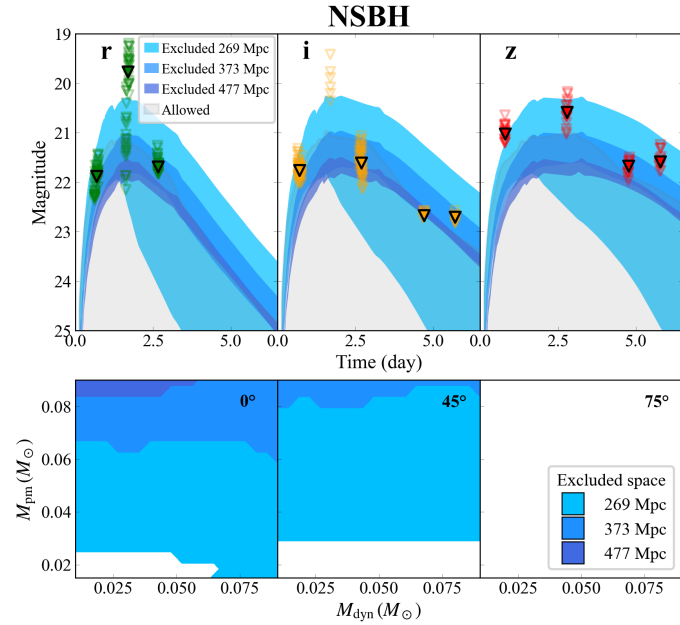


**Figure 6.** Parameters constraint assuming a NSBH merger for S250206dm, similar to Figure 5, but based on the SuperNu KN model. Top and bottom panels show the constraints on simulated KN lightcurves and ejecta masses produced during merger, respectively. The SuperNu NSBH model and three luminosity distances (corresponding to the median and  $\pm 1\sigma$  distances from Bilby skymap) are adopted. Galactic extinction with a median  $E(B - V) = 0.1$  is adopted. In the top panel, the  $5\sigma$  limiting magnitude of each WFST pointing and the median magnitudes are plotted with hollow and solid inverted triangles, respectively. In the bottom panel, three viewing angles of  $0^\circ$ ,  $45^\circ$  and  $75^\circ$  are adopted.

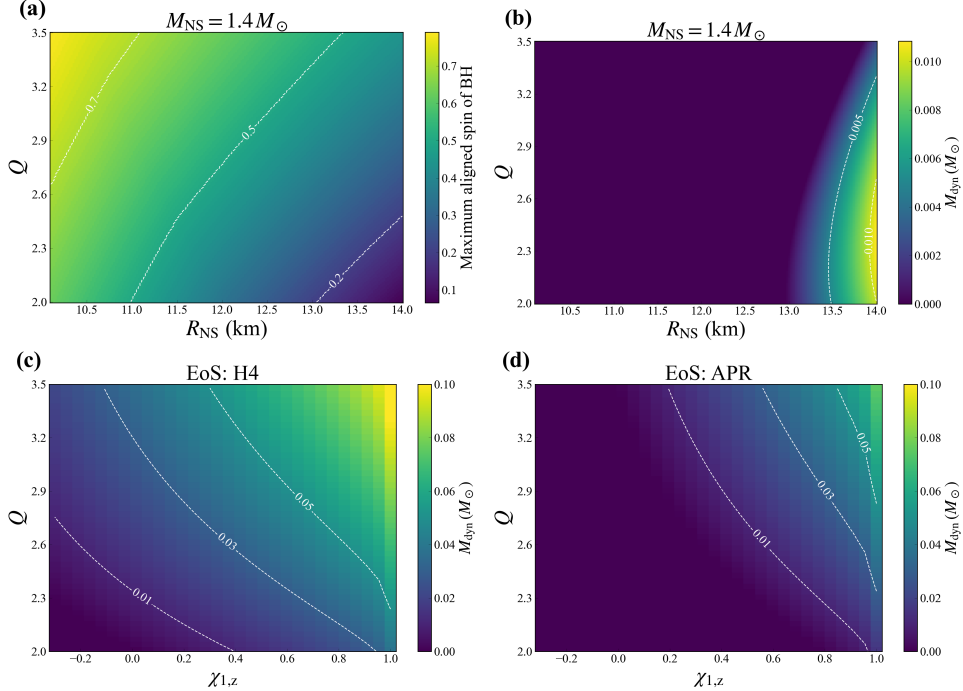


**Figure 7.** The non-detection constraints on the mass ratio ( $Q$ ) and aligned spin of BH ( $\chi_{1,z}$ ) for S250206dm. In Panel (a) and (b), the NS mass is set as  $1.4 M_{\odot}$ , and the white dashed lines represent the contour of allowed maximum aligned spin of BH and the mass of dynamical ejecta, respectively. In Panel (a), the maximum aligned spin of BH derived from ejecta mass limits, where an optimistic result of  $M_{\text{wind}} \lesssim 0.03 M_{\odot}$  and  $M_{\text{dyn}} \lesssim 0.03 M_{\odot}$  is adopted. In Panel (b), a BH with zero aligned spin in system is adopted. In Panel (c) and (d), the EoSs of H4 and APR are adopted to calculate the produced dynamical ejecta mass, respectively. The white dashed lines represent the contour of the mass of dynamical ejecta produced during merger. The system chirp mass is set as  $1.8 M_{\odot}$ , derived from source classification probability of S250206dm.

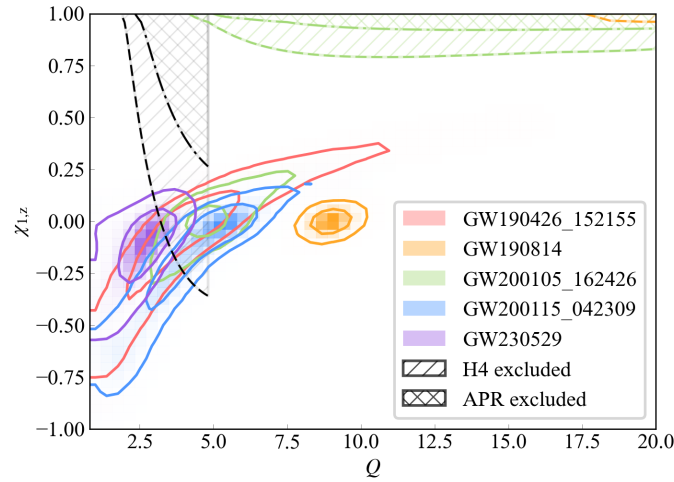


**Figure 8.** The constraints on merger system from optical follow-ups compared with GW posterior estimates. With the chirp mass ( $M_c$ ) fixed, the shaded areas with diagonal and cross represent the excluded spaces of the mass ratio ( $Q$ ) and aligned spin of BH ( $\chi_{1,z}$ ) under EoSs of H4 and APR, respectively.  $Q$  is restricted by the minimum NS mass assumed as  $1 M_{\odot}$ . The gray shaded areas are ruled out space for S250206dm in this work, assuming  $M_c$  as  $1.8 M_{\odot}$  and an optimistic constraint of  $M_{\text{dyn}} \lesssim 0.03 M_{\odot}$ . For GW190814 and GW200105\_162426, the constraints are also shown based on the optimistic upper limits on  $M_{\text{dyn}}$  (S. Anand et al. 2020; I. Andreoni et al. 2020) and  $M_c$  estimates (R. Abbott et al. 2021, 2023) of ( $\lesssim 0.001 M_{\odot}$ ,  $6.1 M_{\odot}$ ) and ( $\lesssim 0.02 M_{\odot}$ ,  $3.4 M_{\odot}$ ), respectively. The contours represent the published GW posterior estimates of NSBH candidates in 50% and 90% confidence (R. Abbott et al. 2021, 2023; A. G. Abac et al. 2024).

Derived from WFST observations, the constraints on the aligned spin of the BH ( $\chi_{1,z}$ ) and the system mass ratio ( $Q = M_{\text{BH}}/M_{\text{NS}}$ ) are shown in Figure 7. In Panel (a) and (b), the NS masses are both assumed as  $M_{\text{NS}} = 1.4 M_{\odot}$ . An optimistic result of  $M_{\text{pm}} \lesssim 0.03 M_{\odot}$  and  $M_{\text{dyn}} \lesssim 0.03 M_{\odot}$  is used to derive the upper limit on  $\chi_{1,z}$ , corresponding to  $\theta_{\text{obs}} = 15^\circ$  and  $D_{\text{L}} = 269$  Mpc. The produced dynamical ejecta mass, given the mass ratio and NS radius, is shown in Panel (b), where a BH with zero aligned spin is assumed, according to low aligned spin measurements of BH for most NSBH merger candidates detected to date (see Table 5). Compared with the constraint of  $M_{\text{dyn}} \lesssim 0.03 M_{\odot}$  from the follow-up observations, it is challenging to derive an informative constraint on mass ratio and NS radius only by WFST observations.

When combined with the GW signal, similar results are shown in Panel (c) and (d) of Figure 7, where the system chirp mass is set to  $M_{\text{c}} = 1.8 M_{\odot}$ , estimated from source classification probability of S250206dm using the method in M. Pillas et al. (2025). The method is described as follows: Estimate of source classifications in some GW online search pipelines, such as PyCBC Live, is based on the method in V. Villa-Ortega et al. (2022). Estimation primarily depends on the measurement of the chirp mass, assuming an astrophysical origin of the event, a correct distance estimate, and a point estimate of the source's detector frame chirp mass by template matching. The latest source classifications estimated by PyCBC Live are 37% and 55% for a BNS merger and a NSBH merger, respectively. Therefore, the chirp mass of S250206dm is derived using the inverse process of the method in V. Villa-Ortega et al. (2022), combined with the event distance estimate. Assuming minimum and maximum NS masses of 1 and  $3 M_{\odot}$ , respectively, a source chirp mass of  $\sim 1.8 M_{\odot}$  is estimated for S250206dm. For the H4 (N. K. Glendenning & S. A. Moszkowski 1991) and APR (A. Akmal et al. 1998) EoSs, the region with  $M_{\text{dyn}} \gtrsim 0.03 M_{\odot}$  is excluded based on the observation-derived constraint, indicating that a NSBH with a large mass ratio and a high aligned spin is disfavored by our observations. Even for a BH with a low aligned spin ( $\chi_{1,z} = 0$ ), a large mass ratio ( $Q \gtrsim 3.2$ ) is still disfavored assuming a “stiff” EoS like H4.

To assess the ability of optical follow-ups in constraining the properties of merger systems, we compare the GW posterior distributions of  $\chi_{1,z}$  and  $Q$  with the constraints derived from optical observations as shown in Figure 8. For NSBH mergers involving a massive black hole ( $> 5 M_{\odot}$ ), such as GW190814 and GW200105\_162426, optical data provide limited constraints. In contrast, for events located within the mass gap like S250206dm, WFST observing constraints reach into the GW posterior of most NSBH candidates. This optical-derived constraint achieves, for the first time, a precision comparable to that inferred from the GW signal, thereby complementing the GW estimate. The result shows that follow-up observations with limiting magnitudes of 22–23 mag can effectively constrain the mass ratio, aiding in distinguishing between a heavy BNS and a NSBH system for mass-gap events.

## 6. OTHER TOO OBSERVATIONS AND JOINT CONSTRAINT

Due to its importance and rarity, for S250206dm, ground-based wide-field survey facilities around the world participated in the EM counterpart search (L. Hu et al. 2025; T. Ahumada et al. 2025; K. W. Smith et al. 2025; G. S. H. Paek et al. 2025; R. Stein et al. 2025), such as ZTF and DECam. However, no valid EM counterpart was reported in the community. The information of some published follow-up observations is listed in Table 5, including ZTF (T. Ahumada et al. 2025) and DECam (L. Hu et al. 2025). WFST observations covered a comparable area (64%) to ZTF (68%), but with a detection limit (-16.1 mag) which is  $\sim 1.3$  magnitudes deeper than that of ZTF (-17.4 mag). Although WFST's limiting magnitude is shallower than that of DECam (-15.2 mag), its coverage is more timely and significantly wider compared to DECam, which began  $\sim 6$  days after the GW detection and covered a 10% area. Additionally, at 269 Mpc, AT 2017gfo-like KNe can be excluded only by WFST observations, as shown in Figure 9. To derive the detection efficiency for AT 2017gfo-like KNe at different positions, we performed a quantitative analysis by randomly sampling  $\sim 19,000$  positions (RA, Dec and luminosity distance) according to the Bilby skymap (Ligo Scientific Collaboration et al. 2025) of S250206dm using the `dynesty` sampler (J. Skilling 2004; J. S. Speagle 2020; S. Koposov et al. 2025). Detection is determined by comparing the luminosity of simulated KNe and  $5\sigma$  limiting magnitudes of WFST observations. Under the requirement of at least one detection in any band, the derived detection ratios under conditions without and with Galactic extinction are  $\sim 34\%$  and  $\sim 10\%$ , respectively. Therefore, in terms of both depth and coverage, WFST has been conducted the best follow-up observations of S250206dm to our knowledge, thanks to the powerful capability of WFST and the great observing conditions at Lenghu site (L. Deng et al. 2021).

Combining the results of other ToO observations helps constrain the potential KN counterpart due to complementarity in observation times and covered region of different telescopes. For S250206dm, the ZTF observations effectively supplement the monitoring of the northern skymap one to two days after the merger, when WFST has relatively

**Table 5. Properties of S250206dm and other published NSBH merger events or candidates.**

Event <sup>1</sup>	$m_1$ ( $M_\odot$ )	$m_2$ ( $M_\odot$ )	$\chi_{1z}$	$D_L$ (Mpc)	$M_{\text{dyn}}^2$ ( $M_\odot$ )	$M_{\text{wind}}$ ( $M_\odot$ )	$M_{\text{lim,abs}}^3$ (mag)	$P_c$	Ref
GW190426_152155	$6.2^{+1.8}_{-1.6}$	$1.6^{+0.4}_{-0.3}$	$-0.04^{+0.19}_{-0.29}$	$370^{+180}_{-160}$	—	—	-16.4	52%	M. M. Kasliwal et al. (2020)
GW190814	$24.4^{+0.7}_{-0.6}$	$2.72^{+0.05}_{-0.05}$	$-0.00^{+0.02}_{-0.02}$	$240^{+40}_{-50}$	—	—	-14.9	99%	K. Ackley et al. (2020)
GW191219_163120	$34.7^{+1.3}_{-1.4}$	$1.30^{+0.04}_{-0.03}$	$-0.00^{+0.04}_{-0.05}$	$550^{+250}_{-160}$	—	—	—	—	—
GW200105_162426	$9.6^{+0.6}_{-0.7}$	$2.02^{+0.11}_{-0.09}$	$-0.00^{+0.05}_{-0.06}$	$270^{+120}_{-110}$	—	—	-17.2	52%	S. Anand et al. (2020)
GW200115_042309	$6.3^{+1.3}_{-1.8}$	$1.53^{+0.48}_{-0.20}$	$-0.15^{+0.16}_{-0.38}$	$290^{+150}_{-100}$	—	—	-15.8	22%	S. Anand et al. (2020)
GW230529_181500	$3.8^{+0.51}_{-0.75}$	$1.49^{+0.31}_{-0.15}$	$-0.11^{+0.12}_{-0.19}$	$201^{+102}_{-96}$	—	0.001(−)	-16.0	16%	M. Pillas et al. (2025)
S250206dm <sup>4</sup>									
	3.84	1.20	0		0.029(−)	0.009(0.001)			
	3.19	1.40	0		0.008(−)	0.010(−)			
	2.73	1.60	0	$373^{+104}_{-104}$	—	0.004(−)	-16.1	64%	WFST (this work)
	3.84	1.20	0.8		0.070(0.038)	0.070(0.052)			
	3.19	1.40	0.8		0.035(0.010)	0.087(0.059)			
	2.73	1.60	0.8		0.008(−)	0.089(0.052)			
S250206dm									
							-17.4	68%	ZTF (T. Ahumada et al. 2025)
							-15.2	9.3%	DECam (L. Hu et al. 2025)
							-17.5	4.9%	T80S (L. Hu et al. 2025)

<sup>1</sup> The information of published GW events are from the posterior distribution results in R. Abbott et al. (2021), R. Abbott et al. (2023), and A. G. Abac et al. (2024).

<sup>2</sup> The ejecta mass produced are calculated assuming the EoS of H4(APR).  $R_{1.4}$  and  $M_{\text{TOV}}$  for EoS H4 and APR are (13.7 km,  $2.03 M_\odot$ ) and (11.3 km,  $2.19 M_\odot$ ), respectively. Marker “ $-$ ” represents the produced ejecta less than  $1 \times 10^{-3} M_\odot$ .

<sup>3</sup> The best median limiting magnitudes from multiple bands and the first three nights are adopted. The median limiting magnitude of DECam on the seventh night is adopted, as observations began on that night.

<sup>4</sup> The chirp mass of  $\sim 1.8 M_\odot$  is adopted, estimated based on the source classification probability of S250206dm (see Materials and Methods). Assuming a non-rotating NS,  $M_{\text{TOV}}$  is used to distinguish between NS and BH in our calculations.

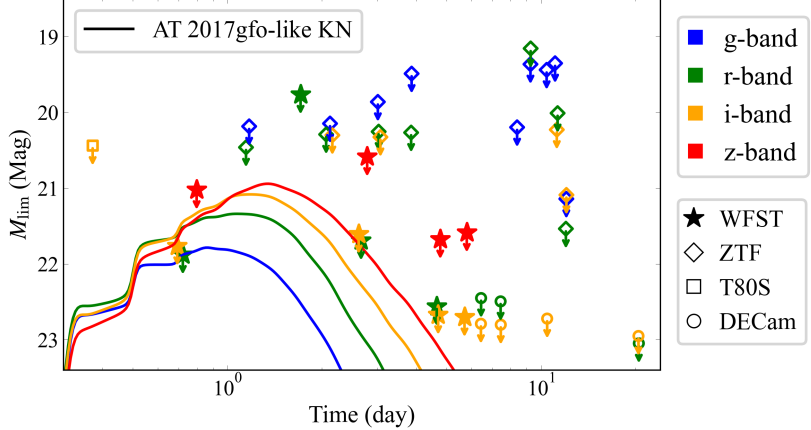


**Figure 9.** Survey depths of WFST and other optical wide-field survey facilities for S250206dm. Lightcurves of AT 2017gfo-like KNs at 269 Mpc and median apparent  $5\sigma$  limiting magnitudes in different bands are represented by solid lines and scatter, respectively. The ZTF data are reported in T. Ahumada et al. (2025), and the T80S and DECam data are reported in L. Hu et al. (2025). Although the regions covered by DECam and T80S focus on the skymap in the southern sky and do not overlap with ZTF and WFST, their depths are also plotted for comparison. Galactic extinction is not considered here.

shallow depth due to cloudy weather (as shown in Figure 9). Combined with ZTF data, the joint constraints on the KN luminosity for BNS and NSBH mergers are shown in Panel (a) and (b) in Figure 10 in the appendix, respectively. For the BNS merger, some bright scenarios are excluded by the ZTF data. The strengthening of constraint is limited for both BNS and NSBH merges due to the difference in depth between WFST and ZTF. Additionally, the joint constraint combining with DECam and T80S data is inappropriate due to the lack of overlap in the covered region with WFST. However, these observations increase the reliability (covered probability increases from 64% to 74%) of the assumption in the model constraint that the merger occurred within the observed field.

## 7. CONCLUSION

In this work, we conducted timely follow-up observations by WFST and detailed EM counterpart search for the GW event S250206dm, which is the first well-localized neutron star merger candidate potentially located in the mass gap. Lasting for a week, WFST observations covered  $\sim 64\%$  of the localization region in  $r$ ,  $i$ ,  $z$  bands with a  $5\sigma$  limiting magnitude up to 23 mag. After data reduction and candidate search, 12 off-nucleus extragalactic transients are discovered, but they are unlikely to be the KN or the afterglow related to S250206dm based on the analysis of host and photometric evolution. Compared with other ToO observations, the WFST follow-up for S250206dm is superior in both depth and coverage.

According to the observation limit, an AT 2017gfo-like KN counterpart to S250206dm at 267 Mpc can only be excluded by WFST. Combined with the KN model POSSIS, the ejecta mass is constrained as:  $M_{\text{pm}} \lesssim 0.03 M_{\odot}$  and  $M_{\text{dyn}} \lesssim 0.01 M_{\odot}$  for a BNS merger;  $M_{\text{pm}} \lesssim 0.03 M_{\odot}$  and  $M_{\text{dyn}} \lesssim 0.03 M_{\odot}$  for a NSBH merger, assuming the condition of a near on-axis observation and at 269 Mpc. Furthermore, the mass ratio of progenitor and aligned spin of BH are also constrained for NSBH merger. Compared with the estimate from GW signal, the constraint on the mass ratio through the optical follow-up can reach the similar order in accuracy for the first time. Our results show that rapid, deep follow-up observations are capable for constraining the properties of compact binary progenitors, providing crucial constraints on the nature of the mass gap.

The WFST observations of S250206dm indicate the potential capacity of WFST in searching for a KN counterpart (Z.-Y. Liu et al. 2023). Due to its unique geographical location, WFST can enhance the counterpart search of GW skymaps in the Northern Hemisphere. Combining with ZTF and Pan-STARRS, WFST is able to complement the wide-field survey facilities in the Southern Hemisphere, such as DECam and LSST. Looking forward, with the participation of WFST and LSST in GW EM counterpart search in upcoming O5<sup>15</sup>, breakthroughs on compact binary merger within mass gap are expected to be achieved.

<sup>15</sup> <https://observing.docs.ligo.org/plan/>

## AUTHOR CONTRIBUTIONS

Z.Y.L. conducted most of the analyses and wrote the manuscript under the supervision of W.Z.. W.Z., Z.P.J., and Z.G.D. initiated this study. Z.L.X., J.A.J., L.L.F., M.X.C., and L.H. contributed to the data reduction pipeline of Wide Field Survey Telescope (WFST). J.A.J., Z.Y.L., Z.L.X., W.Y.W., D.Z.M., J.H.Z., K.X.Y., and Z.Q.J. contributed to the human inspection of the candidate search. R.D.L., L.H., J.J.G., and D.X. helped and discussed the model analyses. T.G.W., X.K., X.F.W., Q.F.Z., Y.Q.X., J.A.J., N.J., Y.X.Z., H.F.Z., M.L., D.Z.Y., B.L., X.Z.Z., F.L., H.L., X.L.Z., J.L.T., H.R.W., Z.W., and J.W. contributed to the development of WFST. All of the authors contributed to the discussion.

## ACKNOWLEDGMENTS

The Wide Field Survey Telescope (WFST) is a joint facility of the University of Science and Technology of China, Purple Mountain Observatory. We appreciate the members of the WFST operation and maintenance team for their support. WZ is supported by the National Natural Science Foundation of China (Grant No. 12325301 and 12273035), Strategic Priority Research Program of the Chinese Academy of Science (Grant No. XDB0550300), the National Key R&D Program of China (Grant No. 2021YFC2203102 and 2022YFC2204602), and Cyrus Chun Ying Tang Foundations. The authors also gratefully acknowledge the support provided by National Key Research and Development Program of China (2023YFA1608100).

*Software:* Astropy ([Astropy Collaboration et al. 2013, 2018, 2022](#)); SciPy ([P. Virtanen et al. 2020](#)); Numpy ([C. R. Harris et al. 2020](#)); Matplotlib ([J. D. Hunter 2007](#)); SWarp ([E. Bertin 2010](#)); dustmap ([G. M. Green 2018](#)); ligo.skymap ([L. P. Singer et al. 2016a,b](#)); HOTPANTS ([A. Becker 2015](#)); afterglowpy ([G. Ryan et al. 2020](#)); dynesty ([J. Skilling 2004; J. S. Speagle 2020; S. Koposov et al. 2025](#))

## APPENDIX

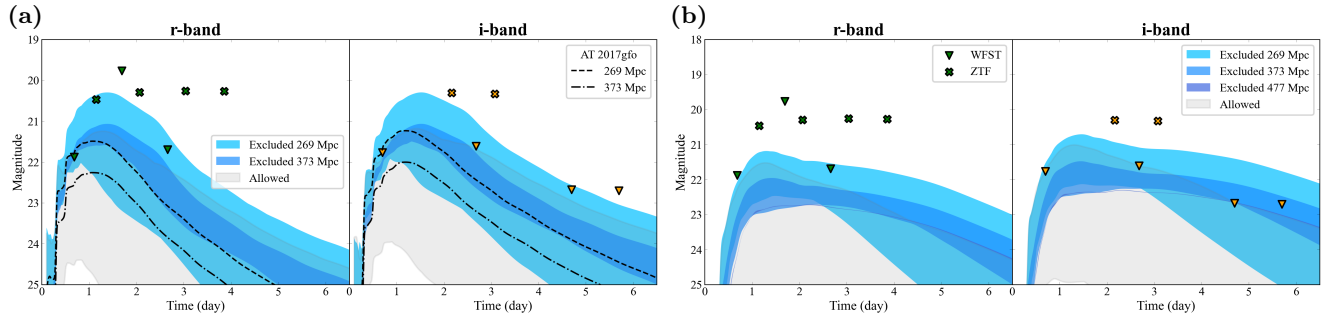


**Figure 10.** Joint constraints on KN luminosity, similar to top two panels in Figure 5, but combining ZTF observations. Panel (a) and (b) correspond to BNS and NSBH mergers, respectively. The median limiting magnitudes of WFST and ZTF are represented by marks of inverted triangle and cross, respectively.

**Table 6. The cross-checked results of reported candidates based on WFST follow-up data.**

TNS Name <sup>1</sup>	Ra	Dec	Coverage	Detection	Team
AT 2025bcq	36.31265	50.17796	Yes	Yes	ZTF
AT 2025bda	354.33854	22.97904	No	No	ZTF
AT 2025bay	7.504874	37.16833	Yes	No	ZTF
AT 2025brm	359.26723	29.48768	Yes	Yes	ZTF
AT 2025ben	356.32103	28.02299	Yes	Yes	ZTF
AT 2025bro	356.59715	28.65744	Yes	No	ZTF
AT 2025brn	2.03711	32.84554	Yes	No	ZTF
AT 2025bcx	7.35227	38.69038	Yes	No	ZTF
AT 2025bcw	21.33198	45.27197	Yes	No	ZTF
AT 2025brp	358.69192	32.65047	Yes	No	ZTF
AT 2025brl	1.90744	27.96404	Yes	Yes	ZTF
AT 2025bcr	20.49131	48.97043	No	No	ZTF
AT 2025bew	31.57170	53.01039	Yes	No	Pan-STARRS
AT 2025bey	25.75487	45.46341	No	No	Pan-STARRS
AT 2025bex	24.46251	45.33960	No	No	Pan-STARRS
AT 2025bev	30.24625	52.32467	Yes	No	Pan-STARRS
AT 2025bcc	32.02902	55.34248	Yes	No	Pan-STARRS
AT 2025bbt	45.46907	51.12973	No	No	Pan-STARRS
AT 2025bbo	24.32197	45.72550	Yes	No	Pan-STARRS
AT 2025bbn	37.78844	50.73533	Yes	No	Pan-STARRS
AT 2025bbm	36.96265	49.47591	Yes	No	Pan-STARRS
AT 2025bw1	357.78800	34.19678	No	No	Pan-STARRS
AT 2025bce	31.23239	54.79534	Yes	No	Pan-STARRS
AT 2025bbl	7.12748	33.19370	No	No	Pan-STARRS
AT 2025bmq	38.51758	54.57247	Yes	Yes	WL-GW
AT 2025azn	39.82257	49.57253	Yes	No	SAGUARO
AT 2025azm	2.03128	32.56575	Yes	No	SAGUARO

<sup>1</sup> The candidates with  $\text{Dec} \leq 0^\circ$  are not included, which are far from the region covered by WFST.

## REFERENCES

Abac, A. G., Abbott, R., Abouelfettouh, I., et al. 2024, The Astrophysical Journal Letters, 970, L34, doi: [10.3847/2041-8213/ad5beb](https://doi.org/10.3847/2041-8213/ad5beb)

Abbott, B. P., Abbott, R., Abbott, T. D., et al. 2017a, The Astrophysical Journal, 848, L12, doi: [10.3847/2041-8213/aa91c9](https://doi.org/10.3847/2041-8213/aa91c9)

Abbott, B. P., Abbott, R., Abbott, T. D., et al. 2017b, Physical Review Letters, 119, 161101, doi: [10.1103/PhysRevLett.119.161101](https://doi.org/10.1103/PhysRevLett.119.161101)

Abbott, B. P., Abbott, R., Abbott, T. D., et al. 2017, Nature, 551, 85, doi: [10.1038/nature24471](https://doi.org/10.1038/nature24471)

Abbott, R., Abbott, T. D., Abraham, S., et al. 2021, Physical Review X, 11, 021053, doi: [10.1103/PhysRevX.11.021053](https://doi.org/10.1103/PhysRevX.11.021053)

Abbott, R., Abbott, T. D., Acernese, F., et al. 2023, Physical Review X, 13, 041039, doi: [10.1103/PhysRevX.13.041039](https://doi.org/10.1103/PhysRevX.13.041039)

Ackley, K., Amati, L., Barbieri, C., et al. 2020, Astronomy & Astrophysics, 643, A113, doi: [10.1051/0004-6361/202037669](https://doi.org/10.1051/0004-6361/202037669)

Ahumada, T., Anand, S., Bulla, M., et al. 2025, arXiv e-prints, doi: [10.48550/arXiv.2507.00357](https://doi.org/10.48550/arXiv.2507.00357)

Akmal, A., Pandharipande, V. R., & Ravenhall, D. G. 1998, Phys. Rev. C, 58, 1804, doi: [10.1103/PhysRevC.58.1804](https://doi.org/10.1103/PhysRevC.58.1804)

Anand, S., Coughlin, M. W., Kasliwal, M. M., et al. 2020, Nature Astronomy, 5, 46, doi: [10.1038/s41550-020-1183-3](https://doi.org/10.1038/s41550-020-1183-3)

Andreoni, I., Goldstein, D. A., Kasliwal, M. M., et al. 2020, The Astrophysical Journal, 890, 131, doi: [10.3847/1538-4357/ab6a1b](https://doi.org/10.3847/1538-4357/ab6a1b)

Astropy Collaboration, Robitaille, T. P., Tollerud, E. J., et al. 2013, A&A, 558, A33, doi: [10.1051/0004-6361/201322068](https://doi.org/10.1051/0004-6361/201322068)

Astropy Collaboration, Price-Whelan, A. M., Sipőcz, B. M., et al. 2018, AJ, 156, 123, doi: [10.3847/1538-3881/aabc4f](https://doi.org/10.3847/1538-3881/aabc4f)

Astropy Collaboration, Price-Whelan, A. M., Lim, P. L., et al. 2022, ApJ, 935, 167, doi: [10.3847/1538-4357/ac7c74](https://doi.org/10.3847/1538-4357/ac7c74)

Barbieri, C., Salafia, O. S., Colpi, M., et al. 2019, The Astrophysical Journal Letters, 887, L35, doi: [10.3847/2041-8213/ab5c1e](https://doi.org/10.3847/2041-8213/ab5c1e)

Beck, R., Szapudi, I., Flewelling, H., et al. 2021, Monthly Notices of the Royal Astronomical Society, 500, 1633, doi: [10.1093/mnras/staa2587](https://doi.org/10.1093/mnras/staa2587)

Becker, A. 2015, HOTPANTS: High Order Transform of PSF ANd Template Subtraction,, Astrophysics Source Code Library, record ascl:1504.004 <http://ascl.net/1504.004>

Bellm, E. C., Kulkarni, S. R., Graham, M. J., et al. 2019, Publications of the Astronomical Society of the Pacific, 131, 018002, doi: [10.1088/1538-3873/aaecbe](https://doi.org/10.1088/1538-3873/aaecbe)

Berthier, J., Vachier, F., Thuillot, W., et al. 2006, in Astronomical Society of the Pacific Conference Series, Vol. 351, Astronomical Data Analysis Software and Systems XV, ed. C. Gabriel, C. Arviset, D. Ponz, & S. Enrique, 367

Bertin, E. 2010, SWarp: Resampling and Co-adding FITS Images Together,, Astrophysics Source Code Library, record ascl:1010.068 <http://ascl.net/1010.068>

Bosch, J., AlSayyad, Y., Armstrong, R., et al. 2018, arXiv e-prints. <http://ascl.net/1812.03248>

Bulla, M. 2019, Monthly Notices of the Royal Astronomical Society, 489, 5037, doi: [10.1093/mnras/stz2495](https://doi.org/10.1093/mnras/stz2495)

Bulla, M. 2023, Monthly Notices of the Royal Astronomical Society, 520, 2558, doi: [10.1093/mnras/stad232](https://doi.org/10.1093/mnras/stad232)

Cai, M., Xu, Z., Fan, L., et al. 2025, arXiv e-prints, doi: [10.48550/arXiv.2501.15018](https://doi.org/10.48550/arXiv.2501.15018)

Chambers, K. C., Magnier, E. A., Metcalfe, N., et al. 2016, arXiv e-prints, arXiv:1612.05560, doi: [10.48550/arXiv.1612.05560](https://doi.org/10.48550/arXiv.1612.05560)

Collaboration, D., Abdul-Karim, M., Adame, A. G., et al. 2025, Data Release 1 of the Dark Energy Spectroscopic Instrument, <https://arxiv.org/abs/2503.14745>

Conroy, G. 2023, Nature, doi: [10.1038/d41586-023-03013-6](https://doi.org/10.1038/d41586-023-03013-6)

Coughlin, M. W., Dietrich, T., Antier, S., et al. 2020, Monthly Notices of the Royal Astronomical Society, 492, 863, doi: [10.1093/mnras/stz3457](https://doi.org/10.1093/mnras/stz3457)

Coulter, D. A., Foley, R. J., Kilpatrick, C. D., et al. 2017, Science, 358, 1556, doi: [10.1126/science.aap9811](https://doi.org/10.1126/science.aap9811)

Dálya, G., Díaz, R., Bouchet, F. R., et al. 2022, Monthly Notices of the Royal Astronomical Society, 514, 1403, doi: [10.1093/mnras/stac1443](https://doi.org/10.1093/mnras/stac1443)

D'Avanzo, P., Campana, S., Salafia, O. S., et al. 2018, Astronomy & Astrophysics, 613, L1, doi: [10.1051/0004-6361/201832664](https://doi.org/10.1051/0004-6361/201832664)

Deng, L., Yang, F., Chen, X., et al. 2021, Nature, 596, 353, doi: [10.1038/s41586-021-03711-z](https://doi.org/10.1038/s41586-021-03711-z)

Dietrich, T., Coughlin, M. W., Pang, P. T. H., et al. 2020, Science, 370, 1450, doi: [10.1126/science.abb4317](https://doi.org/10.1126/science.abb4317)

Eichler, D., Livio, M., Piran, T., & Schramm, D. N. 1989, Nature, 340, 126, doi: [10.1038/340126a0](https://doi.org/10.1038/340126a0)

Flaugher, B., Diehl, H. T., Honscheid, K., et al. 2015, The Astronomical Journal, 150, 150, doi: [10.1088/0004-6256/150/5/150](https://doi.org/10.1088/0004-6256/150/5/150)

Fong, W.-f., Nugent, A. E., Dong, Y., et al. 2022, The Astrophysical Journal, 940, 56, doi: [10.3847/1538-4357/ac91d0](https://doi.org/10.3847/1538-4357/ac91d0)

Förster, F., Cabrera-Vives, G., Castillo-Navarrete, E., et al. 2021, The Astronomical Journal, 161, 242, doi: [10.3847/1538-3881/abe9bc](https://doi.org/10.3847/1538-3881/abe9bc)

Foucart, F., Hinderer, T., & Nissanke, S. 2018, Physical Review D, 98, 081501, doi: [10.1103/PhysRevD.98.081501](https://doi.org/10.1103/PhysRevD.98.081501)

Gaia Collaboration, Vallenari, A., Brown, A. G. A., et al. 2023, Astronomy & Astrophysics, 674, A1, doi: [10.1051/0004-6361/202243940](https://doi.org/10.1051/0004-6361/202243940)

Gal-Yam, A. 2021, in American Astronomical Society Meeting Abstracts, Vol. 237, American Astronomical Society Meeting Abstracts, 423.05

Gao, H., Zhang, B., Lü, H.-J., & Li, Y. 2017, The Astrophysical Journal, 837, 50, doi: [10.3847/1538-4357/aa5be3](https://doi.org/10.3847/1538-4357/aa5be3)

Glendenning, N. K., & Moszkowski, S. A. 1991, Phys. Rev. Lett., 67, 2414, doi: [10.1103/PhysRevLett.67.2414](https://doi.org/10.1103/PhysRevLett.67.2414)

Goldstein, A., Veres, P., Burns, E., et al. 2017, ApJ, 848, L14, doi: [10.3847/2041-8213/aa8f41](https://doi.org/10.3847/2041-8213/aa8f41)

Gompertz, B. P., Nicholl, M., Smith, J. C., et al. 2023, Monthly Notices of the Royal Astronomical Society, 526, 4585, doi: [10.1093/mnras/stad2990](https://doi.org/10.1093/mnras/stad2990)

Graham, M. J., Kulkarni, S. R., Bellm, E. C., et al. 2019, Publications of the Astronomical Society of the Pacific, 131, 078001, doi: [10.1088/1538-3873/ab006c](https://doi.org/10.1088/1538-3873/ab006c)

Green, G. M. 2018, Journal of Open Source Software, 3, 695, doi: [10.21105/joss.00695](https://doi.org/10.21105/joss.00695)

Harris, C. R., Millman, K. J., van der Walt, S. J., et al. 2020, Nature, 585, 357, doi: [10.1038/s41586-020-2649-2](https://doi.org/10.1038/s41586-020-2649-2)

Hu, L., Wang, L., Chen, X., & Yang, J. 2022, The Astrophysical Journal, 936, 157, doi: [10.3847/1538-4357/ac7394](https://doi.org/10.3847/1538-4357/ac7394)

Hu, L., Cabrera, T., Palmese, A., et al. 2025, The Astrophysical Journal Letters, 990, L46, doi: [10.3847/2041-8213/adfd49](https://doi.org/10.3847/2041-8213/adfd49)

Hunter, J. D. 2007, Computing in Science & Engineering, 9, 90, doi: [10.1109/MCSE.2007.55](https://doi.org/10.1109/MCSE.2007.55)

Kasen, D., Metzger, B., Barnes, J., Quataert, E., & Ramirez-Ruiz, E. 2017, Nature, 551, 80, doi: [10.1038/nature24453](https://doi.org/10.1038/nature24453)

Kasliwal, M. M., Anand, S., Ahumada, T., et al. 2020, The Astrophysical Journal, 905, 145, doi: [10.3847/1538-4357/abc335](https://doi.org/10.3847/1538-4357/abc335)

Kawaguchi, K., Shibata, M., & Tanaka, M. 2020, The Astrophysical Journal, 889, 171, doi: [10.3847/1538-4357/ab61f6](https://doi.org/10.3847/1538-4357/ab61f6)

Kedia, A., Ristic, M., O'Shaughnessy, R., et al. 2023, Physical Review Research, 5, 013168, doi: [10.1103/PhysRevResearch.5.013168](https://doi.org/10.1103/PhysRevResearch.5.013168)

Koposov, S., Speagle, J., Barbary, K., et al. 2025, joshspeagle/dynesty: v3.0.0, v3.0.0 Zenodo, doi: [10.5281/zenodo.1726824](https://doi.org/10.5281/zenodo.1726824)

Korobkin, O., Wollaeger, R., Fryer, C., et al. 2021, The Astrophysical Journal, 910, 116, doi: [10.3847/1538-4357/abe1b5](https://doi.org/10.3847/1538-4357/abe1b5)

Krüger, C. J., & Foucart, F. 2020, Physical Review D, 101, 103002, doi: [10.1103/PhysRevD.101.103002](https://doi.org/10.1103/PhysRevD.101.103002)

Lattimer, J. M., Mackie, F., Ravenhall, D. G., & Schramm, D. N. 1977, ApJ, 213, 225, doi: [10.1086/155148](https://doi.org/10.1086/155148)

Lattimer, J. M., & Schramm, D. N. 1974, ApJL, 192, L145, doi: [10.1086/181612](https://doi.org/10.1086/181612)

Li, D. Y., Hu, J. W., Wu, Q. Y., et al. 2025, GRB Coordinates Network, 39545, 1

Ligo Scientific Collaboration, VIRGO Collaboration, & Kagra Collaboration. 2025, GRB Coordinates Network, 39231, 1

Liu, Y., Fan, L., Hu, L., et al. 2025, Astronomy & Astrophysics, 693, A105, doi: [10.1051/0004-6361/202348581](https://doi.org/10.1051/0004-6361/202348581)

Liu, Z.-Y., Lin, Z.-Y., Yu, J.-M., et al. 2023, The Astrophysical Journal, 947, 59, doi: [10.3847/1538-4357/acc73b](https://doi.org/10.3847/1538-4357/acc73b)

Liu, Z. Y., He, L., Zhao, W., et al. 2025, GRB Coordinates Network, 39249, 1

Lukošiute, K., Raaijmakers, G., Doctor, Z., Soares-Santos, M., & Nord, B. 2022, Monthly Notices of the Royal Astronomical Society, 516, 1137, doi: [10.1093/mnras/stac2342](https://doi.org/10.1093/mnras/stac2342)

Magnier, Eugene. A., Schlafly, Edward. F., Finkbeiner, D. P., et al. 2020, The Astrophysical Journal Supplement Series, 251, 6, doi: [10.3847/1538-4365/abb82a](https://doi.org/10.3847/1538-4365/abb82a)

Metzger, B. D. 2020, Living Reviews in Relativity, 23, 1, doi: [10.1007/s41114-019-0024-0](https://doi.org/10.1007/s41114-019-0024-0)

Nakar, E. 2020, Physics Reports, 886, 1, doi: [10.1016/j.physrep.2020.08.008](https://doi.org/10.1016/j.physrep.2020.08.008)

Paek, G. S. H., Im, M., Jeong, M., et al. 2025, GRB Coordinates Network, 39241, 1

Pian, E., D'Avanzo, P., Benetti, S., et al. 2017, Nature, 551, 67, doi: [10.1038/nature24298](https://doi.org/10.1038/nature24298)

Pillas, M., Antier, S., Ackley, K., et al. 2025, arXiv e-prints, doi: [10.48550/arXiv.2503.15422](https://doi.org/10.48550/arXiv.2503.15422)

Planck Collaboration, Aghanim, N., Akrami, Y., et al. 2020, A&A, 641, A6, doi: [10.1051/0004-6361/201833910](https://doi.org/10.1051/0004-6361/201833910)

Raaijmakers, G., Nissanke, S., Foucart, F., et al. 2021, The Astrophysical Journal, 922, 269, doi: [10.3847/1538-4357/ac222d](https://doi.org/10.3847/1538-4357/ac222d)

Ryan, G., Eerten, H. v., Piro, L., & Troja, E. 2020, The Astrophysical Journal, 896, 166, doi: [10.3847/1538-4357/ab93cf](https://doi.org/10.3847/1538-4357/ab93cf)

Savchenko, V., Ferrigno, C., Kuulkers, E., et al. 2017, ApJ, 848, L15, doi: [10.3847/2041-8213/aa8f94](https://doi.org/10.3847/2041-8213/aa8f94)

Schlafly, E. F., & Finkbeiner, D. P. 2011, The Astrophysical Journal, 737, 103, doi: [10.1088/0004-637X/737/2/103](https://doi.org/10.1088/0004-637X/737/2/103)

Shappee, B. J., Simon, J. D., Drouet, M. R., et al. 2017, Science, 358, 1574, doi: [10.1126/science.aaq0186](https://doi.org/10.1126/science.aaq0186)

Shingles, L., Smith, K. W., Young, D. R., et al. 2021, Transient Name Server AstroNote, 7, 1

Singer, L. P., Chen, H.-Y., Holz, D. E., et al. 2016a, *The Astrophysical Journal Letters*, 829, L15, doi: [10.3847/2041-8205/829/1/L15](https://doi.org/10.3847/2041-8205/829/1/L15)

Singer, L. P., Chen, H.-Y., Holz, D. E., et al. 2016b, *The Astrophysical Journal Supplement Series*, 226, 10, doi: [10.3847/0067-0049/226/1/10](https://doi.org/10.3847/0067-0049/226/1/10)

Skilling, J. 2004, in *American Institute of Physics Conference Series*, Vol. 735, Bayesian Inference and Maximum Entropy Methods in Science and Engineering: 24th International Workshop on Bayesian Inference and Maximum Entropy Methods in Science and Engineering, ed. R. Fischer, R. Preuss, & U. V. Toussaint (AIP), 395–405, doi: [10.1063/1.1835238](https://doi.org/10.1063/1.1835238)

Smith, K. W., Smartt, S. J., Young, D. R., et al. 2020, *Publications of the Astronomical Society of the Pacific*, 132, 085002, doi: [10.1088/1538-3873/ab936e](https://doi.org/10.1088/1538-3873/ab936e)

Smith, K. W., Angus, C. R., Young, D. R., et al. 2025, GRB Coordinates Network, 39211, 1

Speagle, J. S. 2020, *MNRAS*, 493, 3132, doi: [10.1093/mnras/staa278](https://doi.org/10.1093/mnras/staa278)

Stein, R., Karambelkar, V., Frostig, D., et al. 2025, GRB Coordinates Network, 39256, 1

Tanvir, N. R., Levan, A. J., González-Fernández, C., et al. 2017, *The Astrophysical Journal*, 848, L27, doi: [10.3847/2041-8213/aa90b6](https://doi.org/10.3847/2041-8213/aa90b6)

Tonry, J. L., Denneau, L., Heinze, A. N., et al. 2018, *Publications of the Astronomical Society of the Pacific*, 130, 064505, doi: [10.1088/1538-3873/aabadf](https://doi.org/10.1088/1538-3873/aabadf)

Troja, E., Piro, L., Van Eerten, H., et al. 2017, *Nature*, 551, 71, doi: [10.1038/nature24290](https://doi.org/10.1038/nature24290)

Villa-Ortega, V., Dent, T., & Curiel Barroso, A. 2022, *Monthly Notices of the Royal Astronomical Society*, 515, 5718, doi: [10.1093/mnras/stac2120](https://doi.org/10.1093/mnras/stac2120)

Virtanen, P., Gommers, R., Oliphant, T. E., et al. 2020, *Nature Methods*, 17, 261, doi: [10.1038/s41592-019-0686-2](https://doi.org/10.1038/s41592-019-0686-2)

Wang, T., Liu, G., Cai, Z., et al. 2023, *Science China Physics, Mechanics & Astronomy*, 66, 109512, doi: [10.1007/s11433-023-2197-5](https://doi.org/10.1007/s11433-023-2197-5)

Wollaeger, R. T., Fryer, C. L., Fontes, C. J., et al. 2019, *The Astrophysical Journal*, 880, 22, doi: [10.3847/1538-4357/ab25f5](https://doi.org/10.3847/1538-4357/ab25f5)

Wollaeger, R. T., Fryer, C. L., Chase, E. A., et al. 2021, *The Astrophysical Journal*, 918, 10, doi: [10.3847/1538-4357/ac0d03](https://doi.org/10.3847/1538-4357/ac0d03)

Xu, Z. L., Meng, D. Z., Liu, Z. Y., et al. 2025, GRB Coordinates Network, 39293, 1

Yu, Y.-W., Zhang, B., & Gao, H. 2013, *The Astrophysical Journal*, 776, L40, doi: [10.1088/2041-8205/776/2/L40](https://doi.org/10.1088/2041-8205/776/2/L40)

Zhang, B. 2018, *The Physics of Gamma-Ray Bursts* (Cambridge University Press), doi: [10.1017/9781139226530](https://doi.org/10.1017/9781139226530)